How to cite: *Angew. Chem. Int. Ed.* **2022,** *61,* e202200259
International Edition: doi.org/10.1002/anie.202200259
German Edition: doi.org/10.1002/ange.202200259

Foldamers

Hybrid Pyridine–Pyridone Foldamer Channels as M2-Like Artificial Proton Channels

*Jie Shen, Ruijuan Ye, Zhiwei Liu, and Huaqiang Zeng**

Abstract: Currently, completely abiotic channel systems that concurrently reproduce the high selectivity and high permeation rate of natural protein channels are rare. Here, we provide one such biomimetic channel system, i.e., a novel family of helically folded hybrid amide foldamers that can serve as powerful artificial proton channels to mimic key transport features of the exceptionally selective Matrix-2 (M2) proton channels. Possessing an angstrom-scale tubular pore 3 Å in diameter, these low water permeability artificial channels transport protons at a rate 1.22 and 11 times as fast as gramicidin A and M2 channels, respectively, with exceptionally high selectivity factors of 167.6, 122.7, and 81.5 over Cl^-, Na^+, and K^+ ions. Based on the experimental and computational findings, we propose a novel proton transport mechanism where a proton may create a channel-spanning water chain from two or more short water chains to facilitate its own transmembrane flux via the Grotthuss mechanism.

Introduction

Nature constantly provides a rich source of inspiration for biomimetic chemistry, which aims to create innovative solutions to a variety of complex problems[1] by imitating or even emulating biological functions via purely chemical means. Particularly, biological membrane channels display an exquisite capacity to precisely control directional flows of cognate species (H_2O,[2] K^+,[3] Na^+,[4] Ca^{2+},[5] Cl^-,[6] H^+,[7] etc.). Moreover, their exceptionally high transport selectivity is often seamlessly integrated with high permeation rate, such that it is exceedingly difficult for artificial channel systems to reach comparable highly integrated performance.

At the present time, we are aware of only one artificially created channel system (e.g., an artificial water channel) rejecting both salts (NaCl and KCl) and protons with near-perfect selectivity, a hallmark feature of its natural counterpart aquaporin 1 (AQP1), while concurrently enabling water to be transported 2.5 times as fast as AQP1.[8] Except for this unusual case, the high selectivity seen in other types of biological membrane channels alone has been a recurring daunting challenge to replicate in artificial channels capable of transporting molecular species such as K^+,[9–17] Na^+,[18–20] Cl^-,[21–33] and I^-.[34–37] For instance, while the natural potassium channel KcsA exhibits a K^+/Na^+ selectivity factor of ≥ 10000,[3] only very recently have manmade K^+-channels started to achieve K^+/Na^+ selectivity values, obtained on the basis of single-channel current traces, of 9.8 (in 2017),[12] 14.0[15] and 16.3[16] (in 2020), and 18.2 (in 2021).[17] And to the best of our knowledge, none of the hitherto known artificial Na^+-channels could attain Na^+/K^+ selectivity of >10.

Specific to proton transport, despite the availability of some selective proton carriers (e.g., fatty acids,[38,39] a boronic acid derivative,[40] 2,4-dinitrophenol,[41] niclosamide,[42] and FCCP[43]), artificial proton channels with high selectivity remain largely unexplored. With one recent exception,[44] all known channels capable of proton conduction also transport water[45–48] or ions.[49–51] To be more precise, proton conduction often is the "by-product" of artificial channels designed for water or ion transport. This is in sharp contrast to the high selectivity seen in the homotetrameric influenza Matrix-2 proton channel, which shuttles protons through the channel while rejecting ions (Na^+ and K^+) and even water molecules.[52–55] Our interest to develop artificial proton-selective channels is not only to fill the gap between natural and artificial systems but also driven by their important applications in fabricating proton-exchange membranes for fuel cells[56] or promoting proton-coupled electron transfer reactions including oxygen reductions.[57]

Angstrom-scale organic nanotubes (ONTs) are an emerging class of structurally and functionally exciting molecules.[16,46,58–71] Toward building an angstrom-scale precision cavity, the intramolecularly H-bonded aromatic amide foldamers (HAAFs),[46,62,68,72–83] being the most diversified class among aromatic foldamers conformationally rigidified by noncovalent forces,[84,85] represent one unique yet powerful strategy.[8,37,60–62,86] Featuring a highly predictable folding structure and a cavity size dictated by their constituent helicity codons, these HAAFs could even remain helically folded in water.[87] One main limitation of these HAAFs is that the amide bond forming reactions often proceed with low yields, since the participating amines and carboxylic acids suffer from backbone rigidity-induced low reactivities. This is the prime reason why, except for some seminal contributions by the groups of Huc[62] and Gong,[88] the

[*] Dr. J. Shen, R. Ye, Prof. Dr. H. Zeng
College of Chemistry, Fuzhou University
Fuzhou, Fujian 350116 (China)
E-mail: 2733910004@qq.com
Prof. Dr. Z. Liu
Department of Chemistry & Biochemistry,
Rowan University
201 Mullica Hill Road,
Glassboro, NJ 08028 (USA)

majority of HAAFs have a short helical height of <1 nm,[46,62,68,72–83] which limits the functional applications of these structurally unique and interesting molecules.

Possessing a sizable angstrom-scale cavity, these HAAFs provide a viable solution to creating robust biomimetic artificial channels.[8,37,86] A logical and likely the most preferred approach to prepare long HAAF-based ONTs is to explore one-pot (co)polymerization. This, unfortunately, has also proved to be difficult because of the low reactivities associated with the participating amines and carboxylic acids. Indeed, over the past ten years or so, all hitherto one-pot polymerization endeavors reported by others have yielded only short HAAFs with an average channel length of ≤ 1.1 nm.[60,61]

Here we demonstrate that the unique class of long hybrid polymeric HAAFs **1**–**6** with an average channel length of ≈2.2 or ≈3.4 nm and cavity diameter of ≈3 Å can be rapidly prepared using different types of amide coupling agents, with PyBOP as the only one that gives rise to membrane-spanning polymeric channel **4** with an average length of ≈3.4 nm (Figure 1). Very significantly, **4** functions as an ultrafast and exceptionally selective first-in-class M2-like proton transporter, having high rejection of water and ions (Cl^-, Na^+, and K^+) while transporting protons 22 % and 10 times faster than gramicidin A (gA) and M2 channels, respectively. Even more significantly, such ultrafast and exceptionally selective proton transport is mediated by two or more short water chains that are induced by the very proton to be transported and they transiently become one seamlessly interconnected channel-spanning water chain.

Results and Discussion

One-Pot Synthesis of Channels 1–6

Recently, after screening many different amide coupling agents including BOP, HATU, and HBTU, we found that phosphoryl chloride ($POCl_3$) is the only reagent for one-pot polymerization, successfully generating long pyridine-based HAAFs with 31 repeating units on average and an average length of 2.8 nm. (For the structure, see $\mathbf{P_{31}}$ in Figure 2a.[86]) This is the first time that polymeric HAAFs have been efficiently made as long as 2.8 nm via a one-pot protocol.

Although $POCl_3$ can be applied to prepare polymer $\mathbf{P_{31}}$ 2.8 nm in length,[86] very surprisingly, $POCl_3$ only produced highly insoluble precipitates of unknown identities from helicity codons **A** and **B** (Figure 1a), rather than desired polymeric pyridine–pyridone amide foldamers $(\mathbf{AB})_n$. This finding suggests that different types of H-bonded helicity condons may require their own cognate coupling agents, which is consistent with our earlier conclusion.[89,90] This further encouraged us to scrutinize other coupling agents, such as HATU, HBTU, BOP, PyBOP, TBTU, and DEPBT (Figure 1a and Table 1).

In the typical reaction setup, compounds **A** (0.2 mmol) and **B** (0.2 mmol) were first mixed in a 20 mL reaction vial protected with N_2 gas. The coupling reagent (0.6 mmol), freshly distilled CH_2Cl_2 (10 mL) and DMF (2 mL), and DIEA (*N*,*N*-diisopropylethylamine, 150 µL) were added. The solution was then stirred at room temperature for 2 days. A simple workup yielded $(\mathbf{AB})_n$ type polymeric channels **1**–**6**, made using HATU, HBTU, BOP, PyBOP, TBTU, and DEPBT (Figure 1a), respectively, with yields of 50–65 %.

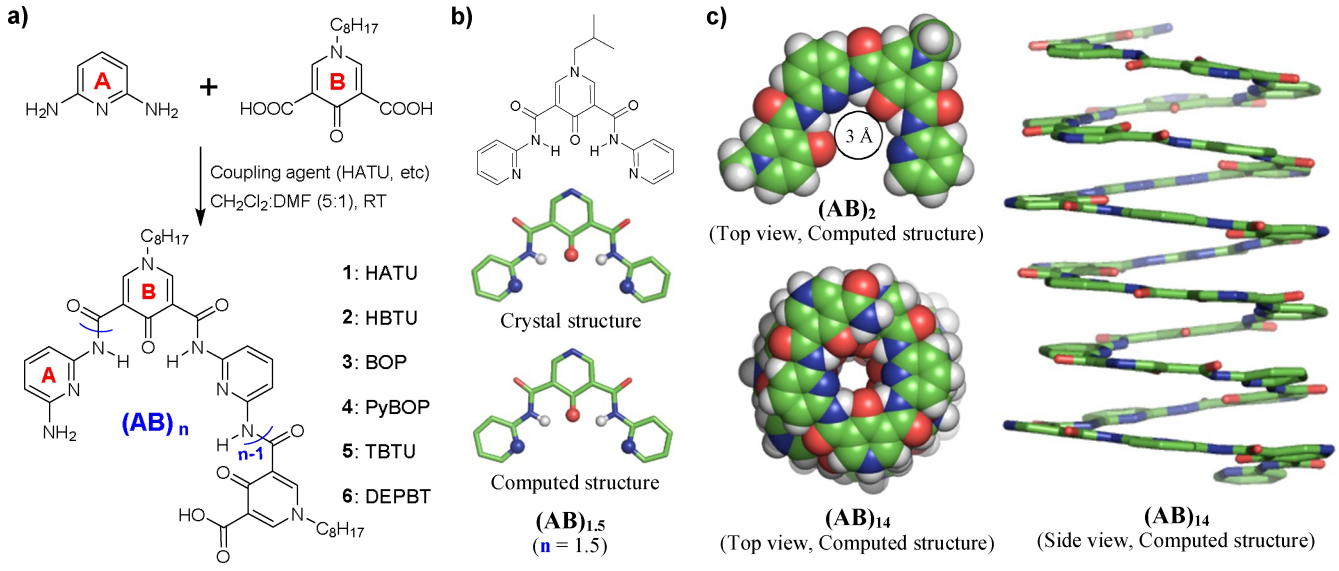

Figure 1. a) One-pot copolymerization of building blocks **A** and **B** to produce polymeric $(\mathbf{AB})_n$ type channels **1**–**6** using the coupling agents HATU, HBTU, BOP, PyBOP, TBTU, and DEPBT, respectively. b) Comparison of the crystal structure (CCDC number 2104777) and the computationally optimized structure for a short oligomer $(\mathbf{AB})_{1.5}$, confirming the high reliability of the computed structures and a pore size of ≈3 Å for $(\mathbf{AB})_2$ and $(\mathbf{AB})_{14}$ presented in (c). Inferred from the computed structure of $(\mathbf{AB})_{14}$: one helical turn requires ≈2.5 **AB** units. The computational method used in (b) and (c) is M06-2X/6-31G(d,p).

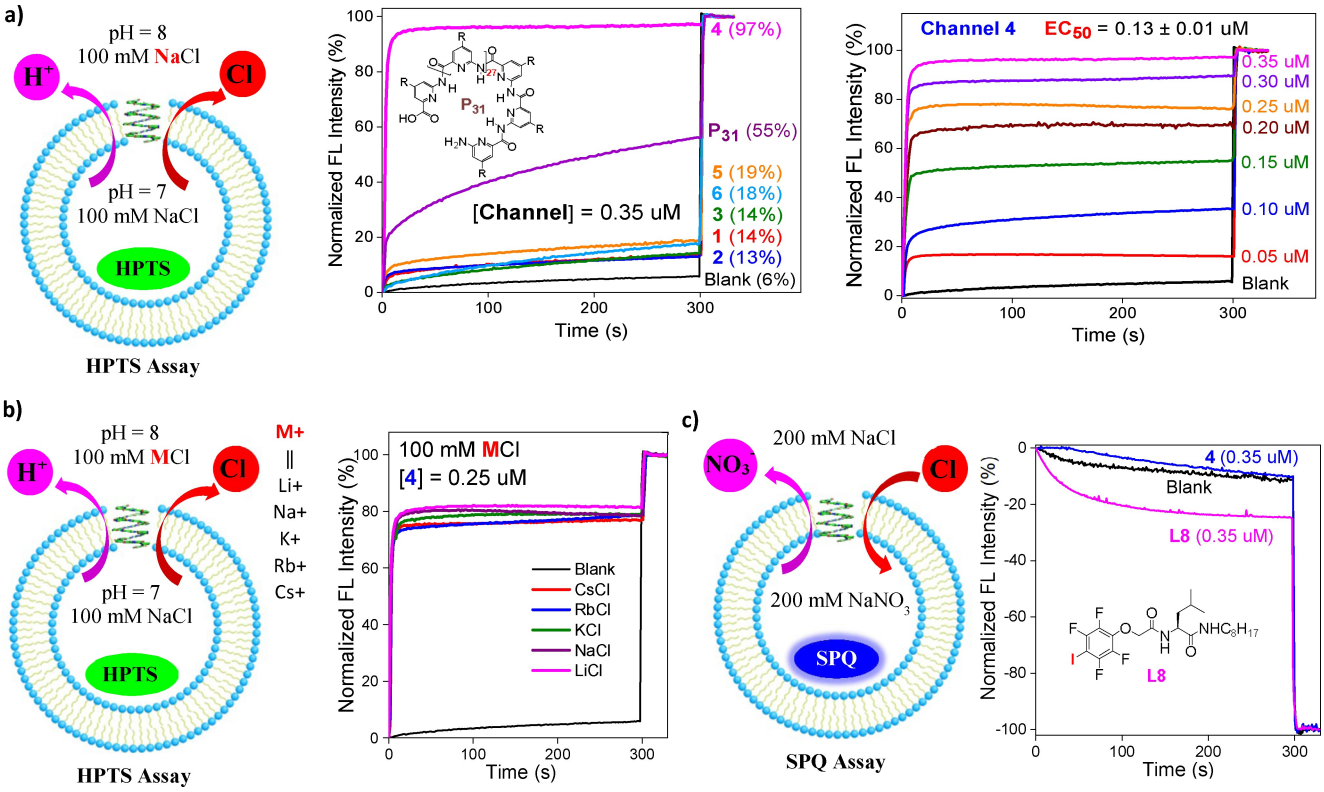

Figure 2. a) The pH-sensitive EYPC-based HPTS assay for gauging ion transport abilities of channels **1**–**6** and for comparison with proton/water channel $\mathbf{P_{31}}$ at 0.35 μM. b) HPTS data that confirm channel **4** does not transport cations. c) Chloride-sensitive EYPC-based SPQ assay, revealing the inability of channel **4** to transport anions. In (a) and (b), fractional proton transport activities, with the extravesicular region containing 100 mM MCl (M = Li, Na, K, Rb, and Cs), were calculated using the equation $R_{H^+} = (I_{H^+} - I_0)/(I_{triton} - I_0)$, wherein I_{H^+} and I_0 (background intensity) are fluorescence emission intensity values at 505 nm with an excitation wavelength of 403 nm (e.g., I_{403}) at $t = 300$ s before addition of triton, and I_{triton} is the corresponding value of I_{403} at $t = 300$ s right after addition of triton. [total lipid] = 50 μM and the size of LUVs is ≈120 nm.

Table 1: GPC data and channel lengths for major GPC peaks[a] of polymers **1**–**6** made using amide coupling reagents.

Channel	Coupling reagents	Mn [KDa]	Area integration [%]	Channel length [nm][b]
1	HATU	5909	99	2.2
2	HBTU	6036	99	2.2
3	BOP	5943	98	2.2
		9281	37	3.4
4	PyBOP	5683 + 5944	63	2.1–2.2
5	TBTU	5988	98	2.2
6	DEPBT	5831	99	2.1

[a] For GPC traces, see Figure S1. [b] Calculated on the basis of MW of 368.44 Da for the **AB** repeating unit and 2.5 such repeating units per helical turn.

PyBOP Generates Membrane-Spanning Channel 4

GPC (gel permeation chromatography) analyses of polymer products **1**–**6** reveal an important difference between polymer **4** and the other polymers (Table 1). Specifically, while 37 % of polymer **4** consists of channels that are made up of 25 **AB** repeating units and are thus 3.4 nm in average channel length, the predominant portions of all other polymers measure 2.1–2.2 nm in length. This difference in polymer product distribution suggests **4** to be likely more active than all other channels since a substantial component of **4** is long enough to span the hydrophobic membrane region. This confirms a unique ability of PyBOP to produce membrane-spanning HAAFs with respect to other amide coupling agents.

Aiming to further increase the proportion of long channels (> 3 nm), our continuing effort will focus on tuning the reaction conditions including temperature, base, DMF content, and type of amide coupling agent.

Channel 4 Exhibits Excellent Proton-Transporting Ability

Although we do not know which ionic species can be transported by channels **1**–**6**, our subsequent analyses do confirm protons to be the main species. The proton transport activities were evaluated by using EYPC-based large unilamellar vesicles (LUVs of ≈120 nm), with the intra- and extravesicular regions set to pH 7 and 8, respectively, to generate a transmembrane proton gradient (see the pH-sensitive HPTS assay in Figure 2a). The measured fractional proton transport activities of channels **1**–**6** at 0.35 μM clearly point to the high proton-transporting capacity of channel **4**. Considering that all the other channels are 2.1–2.2 nm in length and display weak proton transport activities, these comparative data suggest that the longer channels in **4**, having a membrane-spanning length of 3.4 nm, are effective membrane-active channels that facilitate proton transport.

Interestingly, channel **4** also turns out to be considerably more active than the pyridine-based polymer channel $\mathbf{P_{31}}$ with an average channel length of 2.8 nm, which has been shown recently to mediate the fast transport of both water and protons, with a proton transport rate approaching that of gA.[86] From the Hill analysis, the EC_{50} value of **4** was calculated to be 0.13 μM or 0.26 mol % relative to lipids (Figure 2a and Figure S8). Given that membrane-active channels account for about 36.5 % of polymer **4**, the true EC_{50} value should be as low as 0.047 μM or 0.095 mol %.

In addition, the HPTS data obtained by varying the MCl salts (M = Li, Na, K, Rb and Cs) in the extravesicular region reveal insignificant differences in ion transport activity (Figure 2b), confirming that **4** does not transport cations. Using the chloride-sensitive EYPC-based SPQ assay, the fact that the anion transport activity is undetected when compared to anion transporter **F8**[30] (Figure 2c) points to inability of **4** to transport chloride anions.

Channel 4 Transports Protons at an Ultrafast Rate through a Channel Mechanism

In light of its sufficiently long average channel length of 3.4 nm and sufficiently large tubular cavity of 3.0 Å across, it is expected that **4** should transport protons through a channel mechanism. To confirm this hypothesis, we recorded single-channel current traces in a bilayer made up of equal weights of acid-stable glyceryl monooleate and cholesterol for **4**, with both *cis* and *trans* chambers containing 0.25 M HCl (Figure 3a and Figures S11–S13).

From the well-defined single-channel current traces that unambiguously confirm the ability of **4** to mediate transmembrane proton transport at the single-channel level, we obtained proton conduction rate ($\gamma_{H}{}^{+}$) of 252.6 ± 4.0 pS by fitting the *I*–*V* curve using the linear equation of $y = a + b*x$, where slope b is the conductance value ($\gamma_{H}{}^{+}$) in units of nS (Figure 3a). Under identical conditions, the $\gamma_{H}{}^{+}$ value of gA was determined to be 206.3 ± 1.3 pS (Figure 3b and Figure S10), which is 22 % smaller than that of **4**. This is somewhat surprising since gA is well-known for its extraordinarily high ability to transport protons across the membrane via a Grotthuss mechanism. Additionally, based on the conductance values at pH 7 (1.1×10^{-17} A for gA[91] vs 1.2×10^{-18} A for M2 channel[92]), proton transport rate by **4** is roughly 11 times that of M2 channel.

Channel 4 Transports Protons with High Ion Selectivity

Given the small interior cavity of 3.0 Å in **4**, ions such as Na^+, K^+, and Cl^- have to be mostly dehydrated (3–4 water molecules removed), leaving a maximum of two bound water molecules aligned along the channel axis when ions pass through the channel. Further, given that the tubular cavity is periodically and helically decorated by amide H-atoms, pyridine N-atoms, amide H-atoms, and pyridone O-atoms, it is anticipated that the partially positively charged H-atoms will repel cations (e.g., Na^+ and K^+) and electron-rich N- and O-atoms will strongly repel anions (e.g., Cl^-), suggesting that it would be difficult to compensate for the required dehydration energy for 3–4 water molecules. Accordingly, **4** might transport protons preferentially over ions (Na^+, K^+, Cl^-, etc.).

In our effort to determine the H^+/Cl^- transport selectivity (P_{H^+}/P_{Cl^-}), single-channel current traces were recorded for **4** in unsymmetrical baths (*cis* chamber = 0.25 M HCl and *trans* chamber = 0.10 M HCl, Figure 3c and Figure S14). Fitting the *I*–*V* curve in Figure 2c gives a reverse potential value of −46.7 mV (ε_{rev}, Figure 3c). After incorporating the Nernst potential of proton gradient (0.10 M to 0.25 M) and substituting the value of −46.7 mV into a simplified Goldman–Hodgkin–Katz equation (see Figure 3c legend and the Supporting Information for the equation), we obtained an extraordinarily high value of 279.6 as the H^+/Cl^- ion selectivity for **4**.

Substituting the ε_{rev} values −113.0 mV and −123.5 mV (Figure 3d, e, Figures S15 and S16) into equation $\varepsilon_{rev} = RT/F \times \ln(P_M{}^+/P_H{}^+)$ yields exceptionally high H^+/K^+ and H^+/Na^+ selectivity values of 81.5 and 122.7, respectively.

It is worth mentioning that the Cl^- ion, which has a larger ionic diameter (3.5 Å) than the pore diameter of **4** (3.0 Å), turns out to be the least transportable by channel **4**. Compared to Na^+, the fact that K^+ ion is more permeating through channel **4** suggests the dehydration energy (83.0 kcal mol^{-1} for K^+ vs 105.0 kcal mol^{-1} for Na^+) may play a dominant role in determining the H^+/cation selectivity.

Channel 4 Exhibits Negligible Water Transport Activities

As mentioned in the introduction, except for one recent example,[44] all known channels capable of proton conduction also transport water.[45–48] Thus, it is of outstanding interest to investigate the water-transporting potential of **4**, which has been confirmed to transport protons with high preference over ions (Na^+, K^+, and Cl^-). For this purpose, we prepared ≈120 nm LUVs using DOPC (1,2-dioleoyl-*sn*-glycero-3-phosphocholine) and **4** premixed at lipid:channel molar ratios of 6000:1 and 8000:1, with the intravesicular region containing 10 mM HEPES buffer (100 mM NaCl,

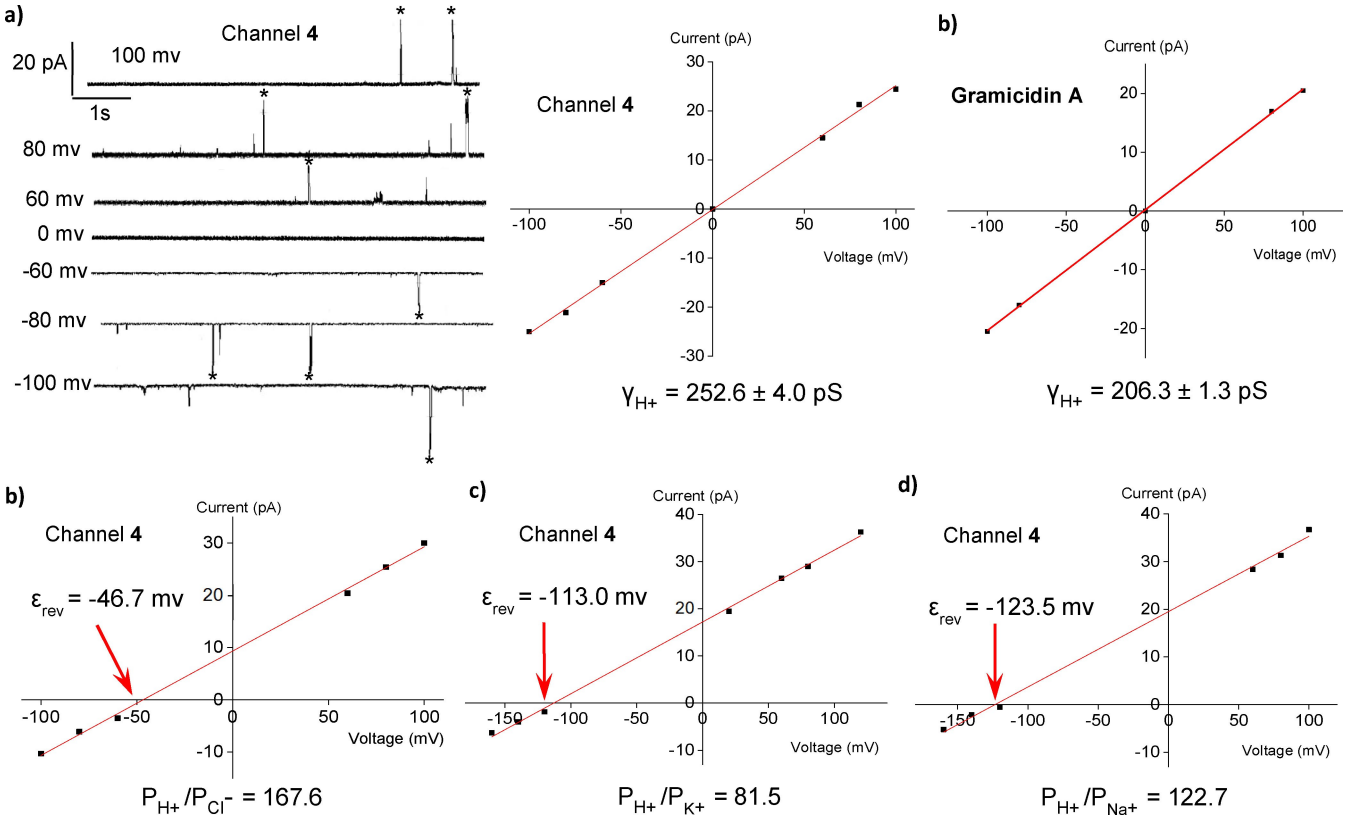

Figure 3. a) Single-channel current traces and current–voltage (*I–V*) curve for channel **4** recorded in a planar lipid bilayer in symmetrical baths (*cis* chamber = *trans* chamber = 0.25 M HCl) from which its proton conduction rate (γ_{H^+}) was determined to be 252.6 ± 4.0 pS; * Symbols refer to current traces used for plotting the *I–V* curve. b) Under the same conditions as in (a), the γ_{H^+} value for gramicidin A was determined to be 206.3 ± 1.3 pS. c–e) *I–V* curves recorded in unsymmetrical baths for determining ion selectivity ratios of P_{H^+}/P_{Cl^-}, P_{H^+}/P_{K^+}, and P_{H^+}/P_{Na^+}. In (a), γ_{H^+} was obtained by fitting the *I–V* curve using the linear equation $y = a + b*x$, where slope b is the conductance value (γ_{H^+}) in units of nS. In (c), the permeability ratio (P_{H^+}/P_{Cl^-}) was calculated using a simplified Goldman–Hodgkin–Katz equation ($\varepsilon_{rev} + 23.5 = RT/F \times \ln\{(P_{H^+} \times [H^+]_{trans} + P_{Cl^-} \times [Cl^-]_{cis})/(P_{H^+} \times [H^+]_{cis} + P_{Cl^-}\,[Cl^-]_{trans})\}$). For (c), (d), the equation for fitting *I–V* curves is $\varepsilon_{rev} = RT/F \times \ln(P_{M^+}/P_{H^+})$. Note that 23.5 mV is the Nernst potential corresponding to a proton gradient from 0.10 M to 0.25 M, R = universal gas constant (8.314 J K^{-1} mol^{-1}), T = 300 K, and F = Faraday's constant (96485 C mol^{-1}).

pH 7.0). Exposing the LUVs to a hypertonic osmolyte having 300 mM sucrose in the same HEPES buffer creates a water concentration gradient (Figure 4). Any water efflux promoted by the concentration gradient only (background signal) or water channels will cause vesicle shrinkage and time-dependent increases in light scattering intensity from which water permeability can be determined.

The insignificant difference in light scattering intensity in the absence (background signal) and the presence of **4** at lipid:channel molar ratios of 6000:1 and 8000:1 (Figure 4 and Figure S17) indicates that **4** does not mediate transmembrane water flux. In fact, the calculated permeability (P_f) value of 120.7 ± 0.4 μm s^{-1} for the blank LUVs turns out to be greater than the P_f values of 104.8 ± 1.4 and 109.1 ± 1.7 μm s^{-1} determined for the LUVs with channel **4** at molar ratios of 6000:1 and 8000:1, respectively. Based on these P_f values over a triplicate run, the calculated water permeability (P_w) in the unit of cm^3 s^{-1} will be negative. This indicates not only that **4** is negligibly active in water transport but also that the alkyl chain-containing rigid structure of **4** tightens the lipid bilayer structure in the way

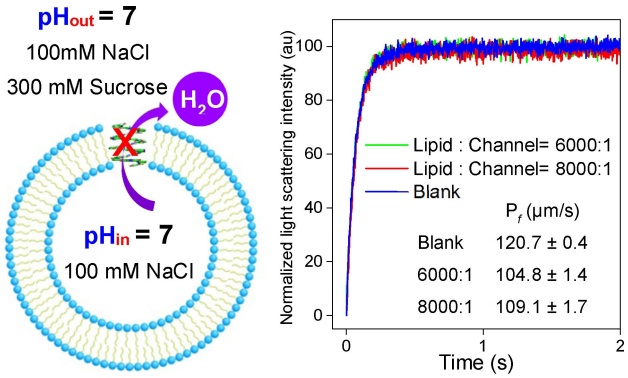

Figure 4. LUV scheme, outlining the hypertonic conditions for investigating the water-transporting potential of **4**. The insignificant differences between the absence and presence of channel molecules and the fact that the P_f value of the blank LUVs is greater than those of the channel-containing LUVs suggest that 1) **4** is negligibly active in water transport and 2) the alkyl chain-containing rigid structure of **4** may make the channel-containing membrane less fluid and less water-permeable than the blank LUVs.

similar to cholesterol, making the membrane less water-permeable than the blank LUVs. The latter phenomenon was also observed for other types of artificial water channels.[8,86,93] In contrast, channel $\mathbf{P_{31}}$ with a length of 2.8 nm, which is a weaker proton transporter than **4**, rapidly transports 1.6×10^9 water molecules per second at a lipid: channel molar ratio of 6000 : 1.[86]

When the lipid:channel molar ratios were kept at 6000 : 1 and 8000 : 1, and a proton gradient of pH 5.3 to 6.5 was applied (Figure S18) or NaCl was replaced with tetrabutylammonium chloride (Figure S19), similar results were obtained. In other words, all the blank LUVs consistently exhibit higher water permeability than the LUVs containing channel **4**.

Proton May Create Its Own Water Wire for Proton Transport

A copious amount of experimental and computational evidence[94,95] supports the notion that protons permeate the membrane through proton channels such as gA by the Grotthuss mechanism.[96] This mechanism refers to the process by which a proton diffuses through an H-bonded water chain at an anomalously fast rate. Currently there are no other alternative mechanisms that can account for proton transport as fast as that observed in gA, the fastest proton transporter among all natural channels.[97]

Since the Grotthuss mechanism requires the formation of a H-bonded water chain and the key functional component of **4** comprises 25 **AB** repeating units on average, we performed molecular dynamics (MD) simulation without an excess proton on a channel molecule $(\mathbf{AB})_{25}$ that contains 25 **AB** repeating units in order to check whether the tubular cavity of $(\mathbf{AB})_{25}$ can accommodate a well-defined single file H-bonded water chain. With optimized torsional parameters for rotation around the aryl–C_{amide} or aryl–N_{amide} bond[98,99] and after MD simulation for 2000 ns, we found that none of the 400000 water-containing structures captured every 5 ps contains a continuously H-bonded water chain as long as 3.4 nm for spanning the whole hollow cavity. Figure 5a illustrates four representative structures at 100, 600, 1000, and 1800 ns. On average, there are about 11.5 water molecules found in $(\mathbf{AB})_{25}$, which can accommodate 15 water molecules, suggesting an average of 24 % empty space per channel. The findings of our current MD simulations can be corroborated by the fact that our previous MD work on structurally similar water/proton-transporting foldamer water channels[86,93] (i.e., $\mathbf{P_{31}}$ shown in Figure 2a[86]) do produce a continuously H-bonded channel-spanning water chain throughout the entire MD trajectory.

The major structural difference between $(\mathbf{AB})_{25}$ having short water chains and $\mathbf{P_{31}}$ having a full channel-spanning water chain is that 50 % of the aromatic units in $(\mathbf{AB})_{25}$ are pyridone units, in which a carbonyl group (C=O) points toward the channel interior and serves as a strong H-bond acceptor. The O-atoms in C=O are roughly 0.5 Å closer to the center of the channel than the N-atoms ($N_{pyridine}$) in the pyridine rings, enabling the formation of bifurcated C=O···H–O–H···O=C or C=O···H–O–H···$N_{pyridine}$ H-bonds. Forming these bifurcated H-bonds re-orientates the water molecule, leaving no water H-atoms available to form the H-bonded water chain. Consistent with this notion, structural analyses over 400000 MD structures confirm that 46.1 % of the water molecules inside the water chain form bifurcated H-bonds (28.4 % for type C=O···H–O–H···O=C, 30.5 % for type C=O···H–O–H···$N_{pyridine}$, and 4.3 % for type $N_{pyridine}$···H–O–H···$N_{pyridine}$, Figure S25). Moreover, 77.6 % of the water molecules at the chain end form bifurcated H-bonds (55.2 %, 49.5 %, and 6.1 % for the three types referenced above, respectively, Figure S25). Note that the sum of the three types is always higher than the overall 46.1 % or 77.6 % since multiple acceptors (C=O or N) H-bond with the same H atom in water (Figure S25). Furthermore, analysis of the MD structures also shows that >99 % of the H-atoms of water molecules at the chain end do not H-bond to the O atoms of the neighboring water

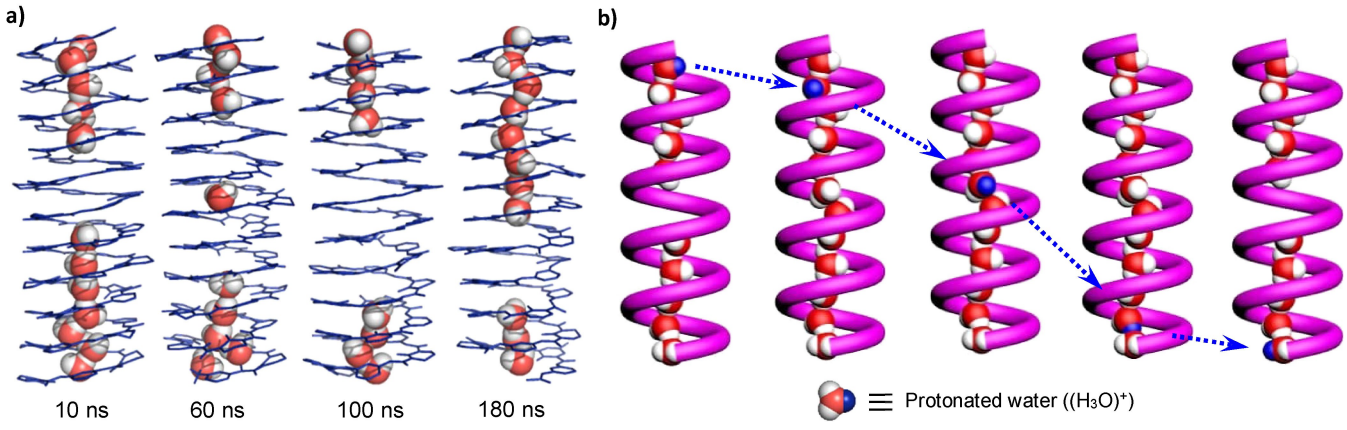

Figure 5. a) MD-simulated water-containing structures at different simulation time points for channel $(\mathbf{AB})_{25}$, which has the 25 **AB** repeating units that are found in the functional component of channel **4**. b) A mechanism for proton transport mediated by channel **4**. In this mechanism, proton transport-induced formation of a continuous H-bonded water chain, which spans the channel, likely is completed by the time the proton moves 2–3 Å (e.g., about one to two water molecules down the pathway) or a slightly longer distance through the channel. And the channel-spanning water chain likely breaks as soon as the proton is 2–3 Å (or slightly further distance) from the exit mouth.

molecules. Instead, they only H-bond (H-bond length: 1.5–3.0 Å; H-bond angle: $>100°$) to the C=O groups and/or $N_{pyridine}$ of the channel molecules (Figure S25). On the other hand, no significant number of bifurcated H-bonds are formed between water and the N-atoms of pyridine rings from $\mathbf{P_{31}}$, and the water molecules trapped in $\mathbf{P_{31}}$ therefore pack in the same way as those in an unconstrained water chain, generating a continuously H-bonded water chain (Figure S25c, d).

As discussed earlier, channel **4** transports protons at a rate 22 % faster than gA. This suggests to us that **4** should also mediate proton transport through the same Grotthuss mechanism. In other words, **4** should be capable of holding a single-file H-bonded water chain, which is contrary to our MD observations. Nevertheless, our MD results are in great accord with the water transport study, revealing the inability of **4** to transport water molecules (Figure 4).

Derived from the Multiscale Reactive MD findings on single-walled carbon nanotubes (CNTs)[100,101] and the M2 proton channel,[102] Voth and his co-workers recently found that the excess proton greatly influences the structural and dynamic changes of the water chain structure. In particular, for an armchair-type (6,6) CNT 29.5 Å in length and with a cavity diameter of 4.7 Å, after excluding the van der Waals radii of carbon atoms, Voth et al. proposed a novel wetting mechanism in which protons create their own water wire, wetting the path ahead for subsequent proton migration via the Grotthuss mechanism.[100] More specifically, by the time protons are 2–3 Å into the tube, the CNT transitions from a partially wet state (e.g., partially H-bonded water chains that do not span the CNT) into a fully wet state (e.g., a fully H-bonded water chain that is as long as the length of CNT).[100]

We believe that Voth's mechanism is equally operative in our artificial proton channel with a cavity diameter of about 3.0 Å (Figure 1c). As elaborated in Figure 5b, **4**-mediated proton transport may involve a few steps. When the proton enters the channel, the number of water molecules on the opposite side may increase, while that on the same side may also increase. As soon as the proton moves 2–3 Å (e.g., about one to two water molecules down the pathway) or slightly further through the channel, the two short H-bonded water chains connect with each other. This creates a fully H-bonded water chain that spans the channel, thus facilitating proton transport to the other side of membrane via the Grotthuss mechanism; this is in contrast to the vehicular transport mechanism where the hydrated proton structure is transported through the pore together as a "nonreactive" hydronium cation.[95] Once the proton is 2–3 Å (or slightly further) from the exit, the water chain likely starts breaking down, returning to the pore to a partially wet state, in which two short H-bonded water chains do not span the channel.

Conclusion

To summarize, among six amide coupling agents tested, PyBOP is the only one that could produce the membrane-spanning and highly active pyridine/pyridone-based amide foldamer channel **4** with an average channel length of 3.4 nm and pore size of 3.0 Å. Channel **4** exhibits excellent proton transport properties, mediating an ultrafast transport of protons at a rate 22 % and 10 times faster than gramicidin A and M2 proton channel, respectively, with high selectivities against ions (Na^+, K^+, and Cl^-) and even water molecules. This high proton transport selectivity makes channel **4** an artificial proton channel that is truly proton-selective and that mimics the key transport features of M2 proton channels. Moreover, channel **4** is the first artificial channel system that highly likely utilizes a proton-induced transiently formed channel-spanning H-bonded water chain to facilitate an ultrafast and exceptionally selective transmembrane proton flux. Artificial proton channels with such high selectivity and permeation rate may find interesting applications in the fabrication of proton-exchange membranes for fuel cells[56] and the promotion of proton-coupled electron transfer reactions including oxygen reductions.[57]

Acknowledgements

This work is supported by Fuzhou University, China and the U.S. National Science Foundation (NSF CHE-1710466).

Conflict of Interest

The authors declare no conflict of interest.

Data Availability Statement

The data that support the findings of this study are available on request from the corresponding author. The data are not publicly available due to privacy or ethical restrictions.

Keywords: Foldamers · Hydrogen Bonds · Organic Nanotubes · Proton Channels · Supramolecular Chemistry

[1] B. Bhushan, *Philos. Trans. R. Soc. A* **2009**, *367*, 1445–1486.
[2] P. Agre, *Angew. Chem. Int. Ed.* **2004**, *43*, 4278–4290; *Angew. Chem.* **2004**, *116*, 4377–4390.
[3] D. A. Doyle, J. Morais Cabral, R. A. Pfuetzner, A. Kuo, J. M. Gulbis, S. L. Cohen, B. T. Chait, R. MacKinnon, *Science* **1998**, *280*, 69–77.
[4] F. H. Yu, W. A. Catterall, *Genome Biol.* **2003**, *4*, 207.
[5] H. Reuter, *Nature* **1985**, *316*, 391.
[6] R. Dutzler, E. B. Campbell, R. MacKinnon, *Science* **2003**, *300*, 108–112.
[7] J. A. Mould, H.-C. Li, C. S. Dudlak, J. D. Lear, A. Pekosz, R. A. Lamb, L. H. Pinto, *J. Biol. Chem.* **2000**, *275*, 8592–8599.
[8] A. Roy, J. Shen, H. Joshi, W. Song, Y.-M. Tu, R. Chowdhury, R. J. Ye, N. Li, C. Ren, M. Kumar, A. Aksimentiev, H. Q. Zeng, *Nat. Nanotechnol.* **2021**, *16*, 911–917.
[9] C. D. Hall, G. J. Kirkovits, A. C. Hall, *Chem. Commun.* **1999**, 1897–1898.

[10] Z. Sun, M. Barboiu, Y.-M. Legrand, E. Petit, A. Rotaru, *Angew. Chem. Int. Ed.* **2019**, *58*, 14539–14543; *Angew. Chem.* **2019**, *131*, 14681–14685.

[11] Z. Sun, A. Gilles, I. Kocsis, Y.-M. Legrand, E. Petit, M. Barboiu, *Chem. Eur. J.* **2016**, *22*, 2158–2164.

[12] C. L. Ren, J. Shen, H. Q. Zeng, *J. Am. Chem. Soc.* **2017**, *139*, 12338–12341.

[13] C. Lang, X. Deng, F. Yang, B. Yang, W. Wang, S. Qi, X. Zhang, C. Zhang, Z. Dong, J. Liu, *Angew. Chem. Int. Ed.* **2017**, *56*, 12668–12671; *Angew. Chem.* **2017**, *129*, 12842–12845.

[14] M. Barboiu, *Acc. Chem. Res.* **2018**, *51*, 2711–2718.

[15] L. Z. Zeng, H. Zhang, T. Wang, T. Li, *Chem. Commun.* **2020**, *56*, 1211–1214.

[16] F. Chen, J. Shen, N. Li, A. Roy, R. J. Ye, C. L. Ren, H. Q. Zeng, *Angew. Chem. Int. Ed.* **2020**, *59*, 1440–1444; *Angew. Chem.* **2020**, *132*, 1456–1460.

[17] S. Qi, C. Zhang, H. Yu, J. Zhang, T. Yan, Z. Lin, B. Yang, Z. Dong, *J. Am. Chem. Soc.* **2021**, *143*, 3284–3288.

[18] A. Nakano, Q. Xie, J. V. Mallen, L. Echegoyen, G. W. Gokel, *J. Am. Chem. Soc.* **1990**, *112*, 1287–1289.

[19] G. W. Gokel, A. Mukhopadhyay, *Chem. Soc. Rev.* **2001**, *30*, 274–286.

[20] F. Otis, C. Racine-Berthiaume, N. Voyer, *J. Am. Chem. Soc.* **2011**, *133*, 6481–6483.

[21] P. H. Schlesinger, R. Ferdani, J. Liu, J. Pajewska, R. Pajewski, M. Saito, H. Shabany, G. W. Gokel, *J. Am. Chem. Soc.* **2002**, *124*, 1848–1849.

[22] V. Sidorov, F. W. Kotch, G. Abdrakhmanova, R. Mizani, J. C. Fettinger, J. T. Davis, *J. Am. Chem. Soc.* **2002**, *124*, 2267–2278.

[23] V. Gorteau, G. Bollot, J. Mareda, A. Perez-Velasco, S. Matile, *J. Am. Chem. Soc.* **2006**, *128*, 14788–14789.

[24] X. Li, B. Shen, X.-Q. Yao, D. Yang, *J. Am. Chem. Soc.* **2007**, *129*, 7264–7265.

[25] C. R. Yamnitz, S. Negin, I. A. Carasel, R. K. Winter, G. W. Gokel, *Chem. Commun.* **2010**, *46*, 2838–2840.

[26] A. Vargas Jentzsch, S. Matile, *J. Am. Chem. Soc.* **2013**, *135*, 5302–5303.

[27] T. Saha, S. Dasari, D. Tewari, A. Prathap, K. M. Sureshan, A. K. Bera, A. Mukherjee, P. Talukdar, *J. Am. Chem. Soc.* **2014**, *136*, 14128–14135.

[28] T. Saha, A. Gautam, A. Mukherjee, M. Lahiri, P. Talukdar, *J. Am. Chem. Soc.* **2016**, *138*, 16443–16451.

[29] X. Wei, G. Zhang, Y. Shen, Y. Zhong, R. Liu, N. Yang, F. Y. Al-mkhaizim, M. A. Kline, L. He, M. Li, Z.-L. Lu, Z. Shao, B. Gong, *J. Am. Chem. Soc.* **2016**, *138*, 2749–2754.

[30] C. L. Ren, X. Ding, A. Roy, J. Shen, S. Zhou, F. Chen, S. F. Yau Li, H. Ren, Y. Y. Yang, H. Q. Zeng, *Chem. Sci.* **2018**, *9*, 4044–4051.

[31] C. L. Ren, F. Zeng, J. Shen, F. Chen, A. Roy, S. Zhou, H. Ren, H. Q. Zeng, *J. Am. Chem. Soc.* **2018**, *140*, 8817–8826.

[32] F. Zeng, F. Liu, L. Yuan, S. Zhou, J. Shen, N. Li, H. Ren, H. Q. Zeng, *Org. Lett.* **2019**, *21*, 4826–4830.

[33] W.-L. Huang, X.-D. Wang, Y.-F. Ao, Q.-Q. Wang, D.-X. Wang, *J. Am. Chem. Soc.* **2020**, *142*, 13273–13277.

[34] N. Madhavan, E. C. Robert, M. S. Gin, *Angew. Chem. Int. Ed.* **2005**, *44*, 7584–7587; *Angew. Chem.* **2005**, *117*, 7756–7759.

[35] B. P. Benke, P. Aich, Y. Kim, K. L. Kim, M. R. Rohman, S. Hong, I.-C. Hwang, E. H. Lee, J. H. Roh, K. Kim, *J. Am. Chem. Soc.* **2017**, *139*, 7432–7435.

[36] L. Yuan, J. Shen, R. J. Ye, F. Chen, H. Q. Zeng, *Chem. Commun.* **2019**, *55*, 4797–4800.

[37] A. Roy, H. Joshi, R. J. Ye, J. Shen, F. Chen, A. Aksimentiev, H. Q. Zeng, *Angew. Chem. Int. Ed.* **2020**, *59*, 4806–4813; *Angew. Chem.* **2020**, *132*, 4836–4843.

[38] F. Kamp, J. A. Hamilton, *Proc. Natl. Acad. Sci. USA* **1992**, *89*, 11367–11370.

[39] X. Wu, P. A. Gale, *J. Am. Chem. Soc.* **2016**, *138*, 16508–16514.

[40] Y. Li, E. C. M. Tse, C. J. Barile, A. A. Gewirth, S. C. Zimmerman, *J. Am. Chem. Soc.* **2015**, *137*, 14059–14062.

[41] M. Goldgof, C. Xiao, T. Chanturiya, W. Jou, O. Gavrilova, M. L. Reitman, *J. Biol. Chem.* **2014**, *289*, 19341–19350.

[42] A. Jurgeit, R. McDowell, S. Moese, E. Meldrum, R. Schwendener, U. F. Greber, *PLoS Pathog.* **2012**, *8*, e1002976.

[43] R. Benz, S. McLaughlin, *Biophys. J.* **1983**, *41*, 381–398.

[44] T. Yan, S. Liu, J. Xu, H. Sun, S. Yu, J. Liu, *Nano Lett.* **2021**, *21*, 10462–10468.

[45] M. Barboiu, A. Gilles, *Acc. Chem. Res.* **2013**, *46*, 2814–2823.

[46] B. Gong, Z. Shao, *Acc. Chem. Res.* **2013**, *46*, 2856–2866.

[47] W. Si, L. Chen, X.-B. Hu, G. Tang, Z. Chen, J.-L. Hou, Z.-T. Li, *Angew. Chem. Int. Ed.* **2011**, *50*, 12564–12568; *Angew. Chem.* **2011**, *123*, 12772–12776.

[48] H. Q. Zhao, S. Sheng, Y. H. Hong, H. Q. Zeng, *J. Am. Chem. Soc.* **2014**, *136*, 14270–14276.

[49] C. Lang, W. Li, Z. Dong, X. Zhang, F. Yang, B. Yang, X. Deng, C. Zhang, J. Xu, J. Liu, *Angew. Chem. Int. Ed.* **2016**, *55*, 9723–9727; *Angew. Chem.* **2016**, *128*, 9875–9879.

[50] L. A. Weiss, N. Sakai, B. Ghebremariam, C. Ni, S. Matile, *J. Am. Chem. Soc.* **1997**, *119*, 12142–12149.

[51] M. Barboiu, Y. Le Duc, A. Gilles, P. A. Cazade, M. Michau, Y. Marie Legrand, A. van der Lee, B. Coasne, P. Parvizi, J. Post, T. Fyles, *Nat. Commun.* **2014**, *5*, 4142.

[52] R. Acharya, V. Carnevale, G. Fiorin, B. G. Levine, A. L. Polishchuk, V. Balannik, I. Samish, R. A. Lamb, L. H. Pinto, W. F. DeGrado, M. L. Klein, *Proc. Natl. Acad. Sci. USA* **2010**, *107*, 15075–15080.

[53] J. L. Thomaston, M. Alfonso-Prieto, R. A. Woldeyes, J. S. Fraser, M. L. Klein, G. Fiorin, W. F. DeGrado, *Proc. Natl. Acad. Sci. USA* **2015**, *112*, 14260–14265.

[54] C. Wei, A. Pohorille, *Biophys. J.* **2013**, *105*, 2036–2045.

[55] I. V. Chizhmakov, F. M. Geraghty, D. C. Ogden, A. Hayhurst, M. Antoniou, A. J. Hay, *J. Physiol.* **1996**, *494*, 329–336.

[56] K. A. Mauritz, R. B. Moore, *Chem. Rev.* **2004**, *104*, 4535–4585.

[57] E. C. M. Tse, C. J. Barile, N. A. Kirchschlager, Y. Li, J. P. Gewargis, S. C. Zimmerman, A. Hosseini, A. A. Gewirth, *Nat. Mater.* **2016**, *15*, 754.

[58] M. A. Balbo Block, C. Kaiser, A. Khan, S. Hecht, *Top. Curr. Chem.* **2005**, *245*, 89–150.

[59] S. Doninelli, M. Badoux, A. F. M. Kilbinger in *Bio-inspired Polymers* (Eds.: N. Bruns, A. F. M. Kilbinger), The Royal Society of Chemistry, London, **2016**, pp. 141–220.

[60] D.-W. Zhang, H. Wang, Z.-T. Li, *Macromol. Rapid Commun.* **2017**, *38*, 1700179.

[61] C.-Z. Liu, M. Yan, H. Wang, D.-W. Zhang, Z.-T. Li, *ACS Omega* **2018**, *3*, 5165–5176.

[62] Y. Ferrand, I. Huc, *Acc. Chem. Res.* **2018**, *51*, 970–977.

[63] D. T. Bong, T. D. Clark, J. R. Granja, M. R. Ghadiri, *Angew. Chem. Int. Ed.* **2001**, *40*, 988–1011; *Angew. Chem.* **2001**, *113*, 1016–1041.

[64] S. Matile, *Chem. Soc. Rev.* **2001**, *30*, 158–167.

[65] J. G. Rudick, V. Percec, *Acc. Chem. Res.* **2008**, *41*, 1641–1652.

[66] I. W. Hamley, *Angew. Chem. Int. Ed.* **2014**, *53*, 6866–6881; *Angew. Chem.* **2014**, *126*, 6984–7000.

[67] T. G. Barclay, K. Constantopoulos, J. Matisons, *Chem. Rev.* **2014**, *114*, 10217–10291.

[68] Y. P. Huo, H. Q. Zeng, *Acc. Chem. Res.* **2016**, *49*, 922–930.

[69] T. Shimizu, *Bull. Chem. Soc. Jpn.* **2018**, *91*, 623–668.

[70] J.-L. Schmitt, J.-M. Lehn, *Helv. Chim. Acta* **2003**, *86*, 3417–3426.

[71] J. Zhu, Z. Dong, S. Lei, L. Cao, B. Yang, W. Li, Y. Zhang, J. Liu, J. Shen, *Angew. Chem. Int. Ed.* **2015**, *54*, 3097–3101; *Angew. Chem.* **2015**, *127*, 3140–3144.

[72] Y. Hamuro, S. J. Geib, A. D. Hamilton, *Angew. Chem. Int. Ed. Engl.* **1994**, *33*, 446; *Angew. Chem.* **1994**, *106*, 465.
[73] J. Zhu, R. D. Parra, H. Q. Zeng, E. Skrzypczak-Jankun, X. C. Zeng, B. Gong, *J. Am. Chem. Soc.* **2000**, *122*, 4219–4220.
[74] V. Berl, I. Huc, R. G. Khoury, M. J. Krische, J. M. Lehn, *Nature* **2000**, *407*, 720–723.
[75] B. Gong, *Chem. Eur. J.* **2001**, *7*, 4336–4342.
[76] I. Huc, *Eur. J. Org. Chem.* **2004**, 17–29.
[77] I. Saraogi, A. D. Hamilton, *Chem. Soc. Rev.* **2009**, *38*, 1726–1743.
[78] G. Guichard, I. Huc, *Chem. Commun.* **2011**, *47*, 5933–5941.
[79] K. Yamato, M. Kline, B. Gong, *Chem. Commun.* **2012**, *48*, 12142–12158.
[80] D.-W. Zhang, X. Zhao, J.-L. Hou, Z.-T. Li, *Chem. Rev.* **2012**, *112*, 5271–5316.
[81] W. Q. Ong, H. Q. Zeng, *J. Inclusion Phenom. Macrocyclic Chem.* **2013**, *76*, 1–11.
[82] H. L. Fu, Y. Liu, H. Q. Zeng, *Chem. Commun.* **2013**, *49*, 4127.
[83] B. Gong, H. Q. Zeng, J. Zhu, L. H. Yuan, Y. H. Han, S. Z. Cheng, M. Furukawa, R. D. Parra, A. Y. Kovalevsky, J. L. Mills, E. Skrzypczak-Jankun, S. Martinovic, R. D. Smith, C. Zheng, T. Szyperski, X. C. Zeng, *Proc. Natl. Acad. Sci. USA* **2002**, *99*, 11583–11588.
[84] S. H. Gellman, *Acc. Chem. Res.* **1998**, *31*, 173–180.
[85] D. J. Hill, M. J. Mio, R. B. Prince, T. S. Hughes, J. S. Moore, *Chem. Rev.* **2001**, *101*, 3893–4011.
[86] J. Shen, J. Fan, R. J. Ye, N. Li, Y. Mu, H. Q. Zeng, *Angew. Chem. Int. Ed.* **2020**, *59*, 13328–13334; *Angew. Chem.* **2020**, *132*, 13430–13436.
[87] S. J. Dawson, Á. Mészáros, L. Pethő, C. Colombo, M. Csékei, A. Kotschy, I. Huc, *Eur. J. Org. Chem.* **2014**, 4265–4275.
[88] Y. Zhong, B. Kauffmann, W. Xu, Z.-L. Lu, Y. Ferrand, I. Huc, X. C. Zeng, R. Liu, B. Gong, *Org. Lett.* **2020**, *22*, 6938–6942.
[89] B. Qin, W. Q. Ong, R. J. Ye, Z. Y. Du, X. Y. Chen, Y. Yan, K. Zhang, H. B. Su, H. Q. Zeng, *Chem. Commun.* **2011**, *47*, 5419–5421.
[90] Z. Y. Du, C. L. Ren, R. J. Ye, J. Shen, Y. J. Lu, J. Wang, H. Q. Zeng, *Chem. Commun.* **2011**, *47*, 12488–12490.
[91] M. Akeson, D. W. Deamer, *Biophys. J.* **1991**, *60*, 101–109.
[92] T. I. Lin, C. Schroeder, *J. Virol.* **2001**, *75*, 3647–3656.
[93] J. Shen, R. J. Ye, A. Romanies, A. Roy, F. Chen, C. L. Ren, Z. Liu, H. Q. Zeng, *J. Am. Chem. Soc.* **2020**, *142*, 10050–10058.
[94] S. Cukierman, *Biophys. J.* **2000**, *78*, 1825–1834.
[95] C. Knight, G. A. Voth, *Acc. Chem. Res.* **2012**, *45*, 101–109.
[96] C. J. T. de Grotthuss, *Ann. Chim.* **1806**, *58*, 54–73.
[97] T. E. Decoursey, *Physiol. Rev.* **2003**, *83*, 475–579.
[98] Z. Liu, A. M. Abramyan, V. Pophristic, *New J. Chem.* **2015**, *39*, 3229–3240.
[99] Z. Liu, A. Teslja, V. Pophristic, *J. Comput. Chem.* **2011**, *32*, 1846–1858.
[100] Y. Peng, J. M. J. Swanson, S.-g. Kang, R. Zhou, G. A. Voth, *J. Phys. Chem. B* **2015**, *119*, 9212–9218.
[101] X. Ma, C. Li, A. B. F. Martinson, G. A. Voth, *J. Phys. Chem. C* **2020**, *124*, 16186–16201.
[102] L. C. Watkins, R. Liang, J. M. J. Swanson, W. F. DeGrado, G. A. Voth, *J. Am. Chem. Soc.* **2019**, *141*, 11667–11676.

Manuscript received: January 7, 2022
Accepted manuscript online: April 5, 2022
Version of record online: May 12, 2022